INTERNATIONAL JOURNAL FOR NUMERICAL METHODS IN FLUIDS, VOL. 3, 363–375 (1983)

TURBULENT HEAT TRANSFER VIA THE F.E.M.: HEAT TRANSFER IN ROD BUNDLES

C. TAYLOR, C. E. THOMAS AND K. MORGAN

Department of Civil Engineering, University College of Swansea, Singleton Park, Swansea SA3 3JT Wales

SUMMARY

Heat transfer associated with forced convection between bundles of cylindrical fuel rods is analysed using the finite element method. A subchannel technique is employed and the numerical results are compared with previous experimental and numerical values. The solid and fluid zones are analysed, for temperature distribution, as a single domain.

1. INTRODUCTION

An optimal design of rod bundles with regard to performance and safety requires an accurate prediction of the thermal and flow characteristics of the inter-rod coolant. The present approach uses the finite element method to calculate the temperature and velocity distribution in association with a subchannel analysis.[1] In such an analysis, the bundles are subdivided into several sub-channels, each bounded by a set of rod surfaces and imaginary lines connecting the rod centres (Figure 1).

Numerical predictions using the finite difference method are fairly numerous. The more recent among these are those of Ramm and Johannsen,[2] Meyder,[1] Buleev,[3,4] Nisjing and

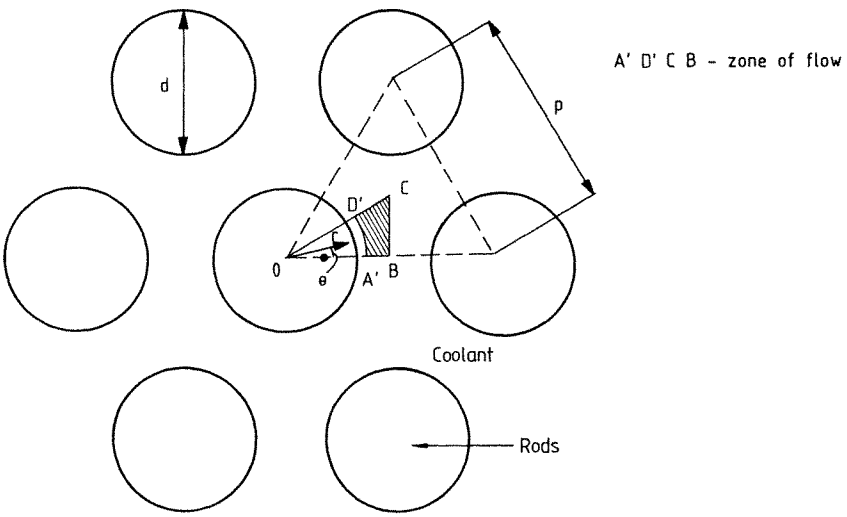

Figure 1. Rod bundle geometry

0271–2091/83/040363–13$01.30

Received 2 June 1982
Revised 16 November 1982

Eifler[5] and Carajilescov and Todreas.[6] The finite element method has been used by Slager[7] and Mikhailov[8] with measurable success. Slager used Meyder's anisotropic mixing length approach and a four noded element and obtained results which agreed favourably with experiment and Meyder's results. Mikhailov, again using four noded elements, used Buleev's approach to solve for both the velocity and temperature distribution within a triangular rod bundle array.

In the present analysis both one and two equation models are used and the results compared with both previously obtained numerical[1,7] and experimental[9] values. In particular, in addition to velocity and temperature distributions a comparison of wall shear stress was also undertaken.

2. GOVERNING EQUATIONS

Although the flow is three dimensional, secondary flows at right angles to the rod axes have been found, both experimentally and numerically, to be negligible relative to the axial flow. The magnitudes of the secondary vortices are, in general, less than 5 per cent of the bulk velocity. Consequently, the present model is restricted to a frequently adopted quasi-three-dimensional approach in which the time averaged velocities, u_1, u_2, in the plane normal to the longitudinal axis of the rods are assumed to be zero. The flow is also considered to be fully developed, and buoyancy terms are ignored. Therefore,

$$\frac{\partial z}{\partial x_3} = 0, \qquad z = u_i, k$$

and

$$\frac{\partial p}{\partial x_3} = \text{constant}$$

in which x_3 is a Cartesian co-ordinate direction parallel to the rod axes, k is the turbulence kinetic energy and p the time averaged local pressure.

The Navier–Stokes equations for turbulent flow involving the above assumptions and the eddy viscosity hypothesis are,

Momentum

$$0 = \frac{\partial p}{\partial x_3} + \frac{\partial}{\partial x_1}\left[(\mu + \mu_T)\frac{\partial u_3}{\partial x_1}\right] + \frac{\partial}{\partial x_2}\left[(\mu + \mu_T)\frac{\partial u_3}{\partial x_2}\right] \tag{1}$$

Continuity

$$\frac{\partial u_1}{\partial x_1} + \frac{\partial u_2}{\partial x_2} + \frac{\partial u_3}{\partial x_3} = 0 \tag{2}$$

Energy

$$u_i \frac{\partial T}{\partial x_i} = \frac{1}{\rho}\frac{\partial}{\partial x_i}\left[\left(\frac{\mu}{\sigma} + \frac{\mu_T}{\sigma_T}\right)\frac{\partial T}{\partial x_i}\right] \tag{3}$$

where μ is the viscosity, μ_T the turbulent viscosity, T the time averaged temperature, σ the Prandtl number and ρ the fluid density. In the energy equation, heat generation due to viscous dissipation has been ignored.

Equation (3) is used to analyse the flow in both the fluid and solid zones. Within a rod the relevant equation is, in the absence of terms associated with velocity, and assuming two

dimensional flow

$$\frac{\partial}{\partial x_1}\left(k_r \frac{\partial T_r}{\partial x_1}\right)+\frac{\partial}{\partial x_2}\left(k_r \frac{\partial T_r}{\partial x_2}\right)+g=0 \tag{4}$$

where the suffix r denotes the rod, k is the thermal conductivity of the rod material and g is the energy source per unit volume.

In the subchannel, the energy equation can now be written,

$$\frac{\partial}{\partial x_1}\left[\left(\frac{\mu}{\sigma}+\frac{\mu_T}{\sigma_T}\right)\frac{\partial T_c}{\partial x_1}\right]+\frac{\partial}{\partial x_2}\left[\left(\frac{\mu}{\sigma}+\frac{\mu_T}{\sigma_T}\right)\frac{\partial T_c}{\partial x_2}\right]=\rho u_3 \frac{\partial T_c}{\partial x_3} \tag{5}$$

Ensuring an overall energy balance between the rod and fluid leads to the following relationship,

$$\frac{\partial}{\partial x_1}\left[\left(\frac{\mu}{\sigma}+\frac{\mu_T}{\sigma_T}\right)\frac{\partial T_c}{\partial x_2}\right]+\frac{\partial}{\partial x_2}\left[\left(\frac{\mu}{\sigma}+\frac{\mu_T}{\sigma_T}\right)\frac{\partial T_c}{\partial x_2}\right]=\frac{u_3}{\bar{u}_3}\frac{A_r}{A_c}\frac{\bar{g}\mu}{k'\sigma} \tag{6}$$

in which,

$$\bar{g}=\frac{1}{A_r}\int_{A_r} g\,dx_1\,dx_2$$

$$\bar{u}_3=\frac{1}{A_c}\int_{A_c} u_3\,dx_1\,dx_2$$

and A_r and A_c are the cross-sectional areas of the rod and coolant, respectively, and k' the effective thermal diffusivity of the fluid.

Equations (4) and (6) now form the equations to be solved across the whole domain provided suitable boundary conditions and spatial distributions of both $g/\bar{g}$ and k_r/k' are known.

The turbulent viscosity can be evaluated from the Prandtl–Kolmogorov relationship

$$\mu_T = C_\mu \rho k^{1/2} l \tag{7}$$

in which C_μ is usually assumed to be constant.

Another model for μ_T is that published by Buleev *et al.*[4] in which,

$$\frac{\mu_T}{\sigma_T}=0{\cdot}2 f_0(\eta) f_1(\eta)\gamma^* \tag{8}$$

and

$$\frac{\mu_T}{\mu\sigma_T}=0{\cdot}2 f_0(\eta) f_1(\lambda\eta)\gamma^* \tag{9}$$

to yield

$$\sigma_T = f_1(\eta)/f_1(\lambda\eta) \tag{10}$$

where

$$\lambda = 0{\cdot}8+0{\cdot}2/\sigma^{0{\cdot}67}, \qquad \sigma<1$$

$$\lambda = 1, \qquad \sigma>1$$

and

$$\gamma^* = \frac{\rho L_1^2}{\mu}\frac{\partial u_3}{\partial n}$$

The length scale L_1 is a function of position which, for the present geometry, is defined at point P (Figure 2) as

$$L = \mathrm{PQ}\left(1{\cdot}0-0{\cdot}5\frac{\mathrm{PQ}}{\mathrm{QS}}\right)$$

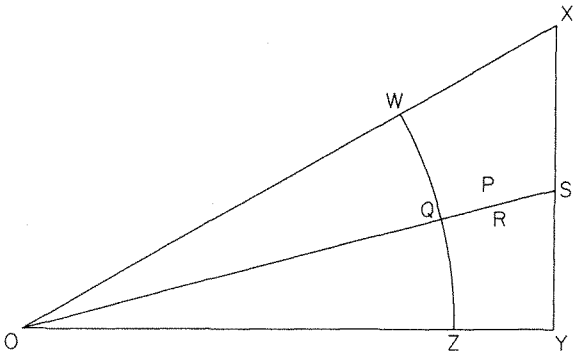

Figure 2. Notation used in the definition of Buleev's length scale

The functions $f_0(\eta)$ and $f_1(\eta)$ are defined by,

$$f_0(\eta) = \exp(-\eta)$$
$$f_1(\eta) = (1-\exp(-\eta))/\eta$$

and

$$\eta = \frac{65}{\gamma^*}$$

The turbulence kinetic energy, k, may be evaluated, in the one equation model of turbulence, from

$$0 = \frac{\partial}{\partial x_1}\left[\left(\mu + \frac{\mu_T}{\sigma_k}\right)\frac{\partial k}{\partial x_1}\right] + \frac{\partial}{\partial x_2}\left[\left(\mu + \frac{\mu_T}{\sigma_k}\right)\frac{\partial k}{\partial x_2}\right] + \mu_T\left[\left(\frac{\partial u_3}{\partial x_1}\right)^2 + \left(\frac{\partial u_3}{\partial x_2}\right)^2\right] - \rho C_D \frac{k^{3/2}}{l} \tag{11}$$

Generally C_D is considered to be constant and the value of the length scale, l, is evaluated algebraically from Reference 6,

$$\left.\begin{aligned} &\frac{l}{\hat{r}} = \frac{r}{\hat{r}}, && 0 < \frac{r}{\hat{r}} < 0{\cdot}44 \\ &\frac{l}{\hat{r}} = 0{\cdot}44 + 0{\cdot}066 \sin\left[\pi \frac{\left(\frac{r}{\hat{r}} - 0{\cdot}44\right)}{0{\cdot}38}\right], && 0{\cdot}44 < \frac{r}{\hat{r}} < 1 \end{aligned}\right\} \tag{12}$$

which were verified experimentally. Here $\hat{r}$ is the radial distance from the rod wall to the maximum velocity line and r measured radially from the wall.

In the two equation model (12) is dispensed with and the length scale is obtained from a further equation,

$$0 = \frac{\partial}{\partial x_1}\left[\left(\mu + \frac{\mu_T}{\sigma_\varepsilon}\right)\frac{\partial \varepsilon}{\partial x_1}\right] + \frac{\partial}{\partial x_2}\left[\left(\mu + \frac{\mu_T}{\sigma_\varepsilon}\right)\frac{\partial \varepsilon}{\partial x_2}\right] + C_1 \rho k\left[\left(\frac{\partial u_3}{\partial x_1}\right)^2 + \left(\frac{\partial u_3}{\partial x_2}\right)^2\right] - C_D \rho \frac{\varepsilon^2}{k} \tag{13}$$

where

$$\varepsilon = \frac{k^{3/2}}{l}$$

3. WALL FUNCTIONS

In confined flow, the steep gradients of velocity, turbulent kinetic energy, dissipation rate of turbulence kinetic energy and temperature in the region close to a solid wall usually

necessitate the use of wall functions in order to avoid excessive finite element mesh refinement. The mesh is terminated some distance from the rod surface (hatched area in Figure 1), and the near wall variation in the relevant variables are depicted via algebraic functions. The near wall nodes are placed within the fully turbulent zone which obviates the necessity for wall functions for laminar and transition zones. A set of wall functions that can be used are,

$$\left.\begin{aligned} u_3 &= \frac{1}{K_1}\left(\frac{\tau_W}{\rho}\right)^{1/2} \log_e [Er_+] \\ k &= (C_\mu \tau_w)/(K_1^2 \rho) \\ T_+ &= \sigma_T\left[2{\cdot}5 \log_n \left(\frac{r}{\nu}\sqrt{\frac{\tau_w}{\rho}}\right) + 5{\cdot}5P\left(\frac{\sigma}{\sigma_t}\right)\right] \end{aligned}\right\} \tag{14}$$

in which K and E are constants, τ_w is the local wall shear stress and r is measured radially from the rod surface. The remaining required definitions are

$$\left.\begin{aligned} r_+ &= \left(\frac{r\rho}{\mu}\right)\left(\frac{\tau_w}{\rho}\right) \\ T_+ &= \frac{(T - T_w)}{T_c}\sqrt{\frac{\tau_w}{\rho}} \end{aligned}\right\} \tag{15}$$

and

$$P\left(\frac{\sigma}{\sigma_t}\right) = 9{\cdot}24\left[\left(\left(\frac{\sigma}{\sigma_t}\right)^{3/4} - 1\right) - 1\right]\left[0{\cdot}28 \exp\left(-0{\cdot}007\,\frac{\sigma}{\sigma_t}\right) + 1\right]$$

where T_w is the temperature at the wall, T_c is a constant and $P(\sigma/\sigma_t)$ is the Spalding–Jayatalika function.

The wall shear stress, τ_w, is given by,

$$\tau_w = \mu \left.\frac{\partial u_3}{\partial r}\right|_{\text{wall}} = (\mu + \mu_T) \left.\frac{\partial u_3}{\partial r}\right|_{\text{near wall node}} \tag{16}$$

3.1. *Boundary conditions*

The remaining boundary conditions on surfaces AB, BC and CD are,

$$\frac{\partial u_3}{\partial n} = \frac{\partial k}{\partial n} = \frac{\partial \varepsilon}{\partial n} = \frac{\partial T}{\partial n} = 0$$

where n is the actual normal to the bounding surface. At the rod surface,

$$u_3 = k = 0$$

4. SOLUTION PROCEDURE

The method of solving the momentum and continuity equations has been adequately reported elsewhere.[10,11] The primitive variable approach is adopted and a suitable iteration scheme is adopted. The Galerkin weighted residual approach is used and an eight noded isoparametric finite element employed. An estimate of the near wall boundary values is required to initiate the solution procedure. When the relevant equations have been solved for the current iteration, the wall shear stress can be estimated from (16). Updated estimates for u_3, k and ε can then be obtained and the procedure repeated until convergence is

achieved. All variables were underrelaxed with a relaxation factor of 0·5 and iterations continued until the maximum relative change in the variables was within 1 per cent.

Once the velocity distribution is known then the average velocity,

$$\bar{u} = \frac{1}{A} \int_A u_3 \, dA \tag{17}$$

can be evaluated, where A is the hatched area in Figure 1. The Reynolds number could then be determined from

$$Re = \rho \frac{\bar{u}}{\mu} h \tag{18}$$

where

$$h = 4a/b$$

a is the cross-sectional area of the fluid and b is the wetted perimeter.

Having determined the velocity distribution, equation (3) can be solved, uncoupled from the flow equations, for the distribution of temperature. When the wall function is used then, again, the solution becomes, of necessity, iterative. The near wall temperature boundary is guessed in order to initiate the procedure, and equation (3) solved for T. From this distribution the wall heat flux can be estimated from,

$$q_{\text{wall}} = \left. \frac{\mu_t}{\sigma_t} \frac{dT}{dr} \right|_{\text{near wall node}}$$

Substituting into the assumed wall function (14) should then yield an improved near wall boundary condition on temperature. The procedure is repeated until convergence is obtained. The same relaxation factors and convergence criteria used for the velocity were again used for the temperature.

A dimensionless Nusselt number,

$$Nu = L \frac{\partial T}{\partial x_n} \Big/ (T - T_0) \tag{19}$$

can be evaluated once the temperature distribution is known. Here T_0 is defined as the bulk temperature of the fluid and L a characteristic length.

4.1. *Illustrative example*

The aspect ratio p/d, where p is the distance between the rod centres and d the rod diameter, chosen for the present example is 1·217. The finite element mesh used is shown in Figure 3, and consists of 120 elements and 407 node points. This was found to give results in agreement with very much finer meshes, and considered adequate for present purposes. The physical location of the near wall nodes was chosen so that,

$$r_+ \gg 30{\cdot}0$$

to ensure that these remained in the fully turbulent zone. This ensured that the use of only one wall function was sufficient. For ease of comparison with experimental[9] and numerical[7,1] results, a Reynolds number of 270,000 was chosen.

Using equation (12) to evaluate the distribution of the Prandtl length scale, a comparison is made of the shear stress (Figure 4) between previously published data and the present results.

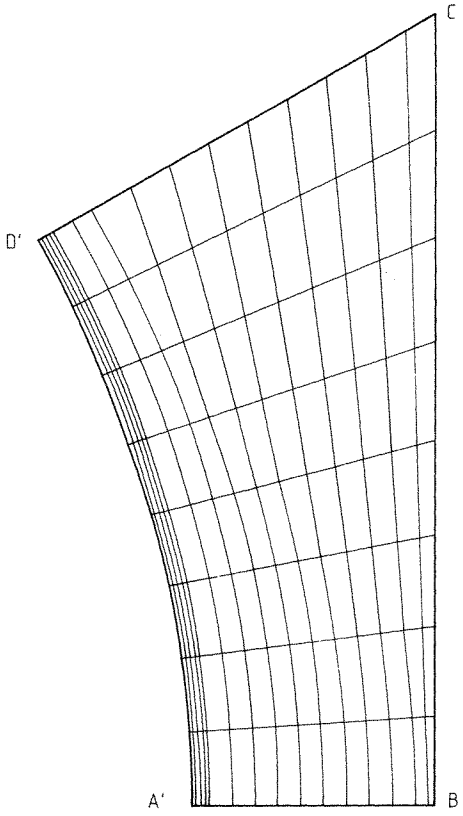

Figure 3. Rod bundle mesh. 120 elements, 407 nodes

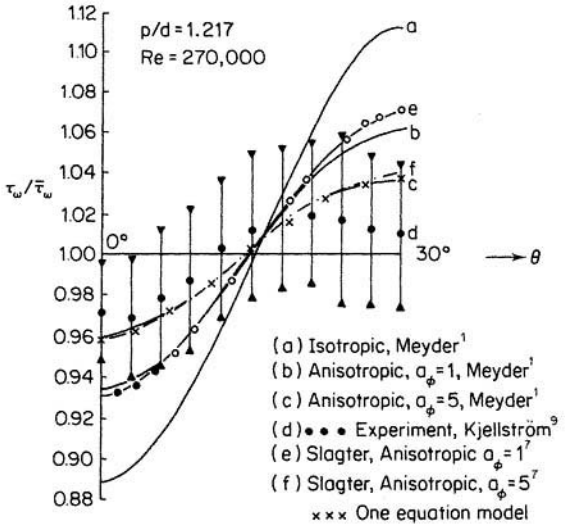

Figure 4

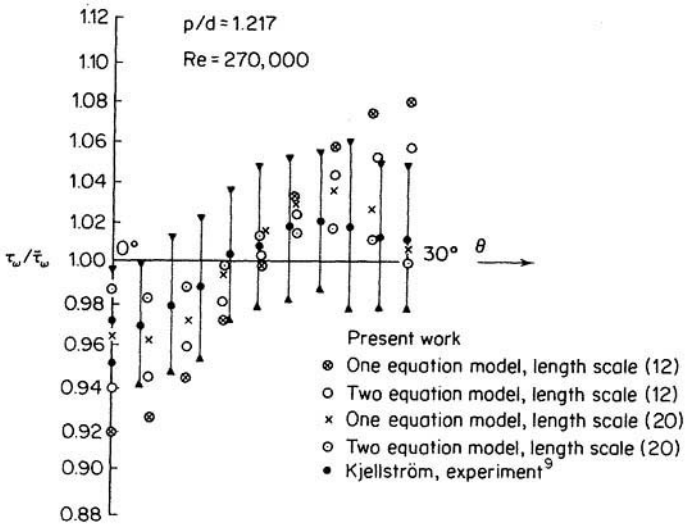

Figure 5

Improved near wall predictions of the wall shear stress and velocity profiles were obtained when a modified distribution of length scale was used. This varies with both radial distance from the rod wall and also with its angular location (Figure 1). The form adopted[6] can be represented by,

$$l = r\left[1{\cdot}25\left(1-\frac{\theta}{30}\right)+\frac{0{\cdot}8928\theta}{30}\right] \qquad 0<\frac{r}{\hat{r}}<0{\cdot}25$$

$$l = 0{\cdot}8928r\frac{\theta}{30}+\hat{r}\left[0{\cdot}3125+0{\cdot}119\sin\left(2\pi\left(\frac{r}{\hat{r}}-0{\cdot}25\right)\right)\right]\left(1-\frac{\theta}{30}\right) \qquad 0{\cdot}25<\frac{r}{\hat{r}}<0{\cdot}4833$$

$$l = \hat{r}\left[0{\cdot}3125+0{\cdot}119\sin\left(2\pi\left(\frac{r}{\hat{r}}-0{\cdot}25\right)\right)\right]\left(1-\frac{\theta}{30}\right)$$
$$+\hat{r}\left[0{\cdot}43152+0{\cdot}10083\sin\left(\left(\frac{r}{\hat{r}}-0{\cdot}4833\right)\left(\frac{3\pi}{2}\Big/0{\cdot}516667\right)\right)\frac{\theta}{30}\right., \qquad 0{\cdot}4833<\frac{r}{\hat{r}}<1 \qquad (20)$$

The variation in shear stress predicted using this length scale, (Figure 5), was significantly better than those obtained previously. Again the velocities tended to be too large approximately midway between the rods and the centreline.

The wall shear stress distribution obtained when the two equation model and modified length scale was considerably better than the one equation model (Figures 5, 6). The results are also compared with previous numerical and experimental values (Figure 7); those obtained using the modified length scale are again acceptable. Some velocity contour plots are presented in Figures 8–10. A comparison of the length scale values is shown in Figure 11 on the 0° and 30° radial extremities. The two equation model follows the same basic shape as those devised by Buleev[3] although they are slightly smaller on the centreline.

The Nusselt number is evaluated in terms of an average temperature defined by,

$$\bar{T} = \frac{1}{A}\int_A T\,\mathrm{d}A \qquad (21)$$

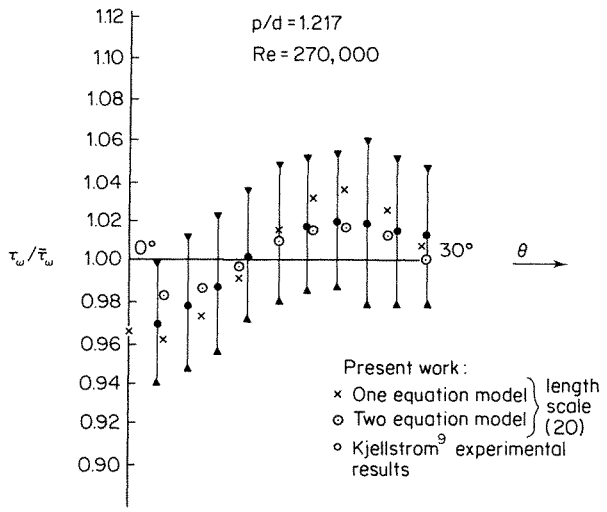

Figure 6

resulting in the Nusselt number,

$$Nu = L\frac{\partial T}{\partial x_n}\Big/(T_s - \bar{T})$$

Although a wall function could have been used for the near wall distribution of temperature it was found, in common with other numerical analyses,[4,8] that an accurate temperature

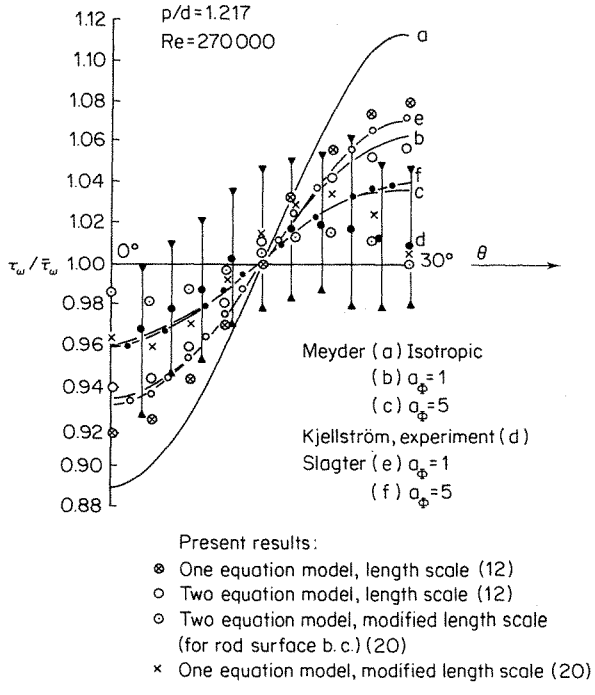

Figure 7

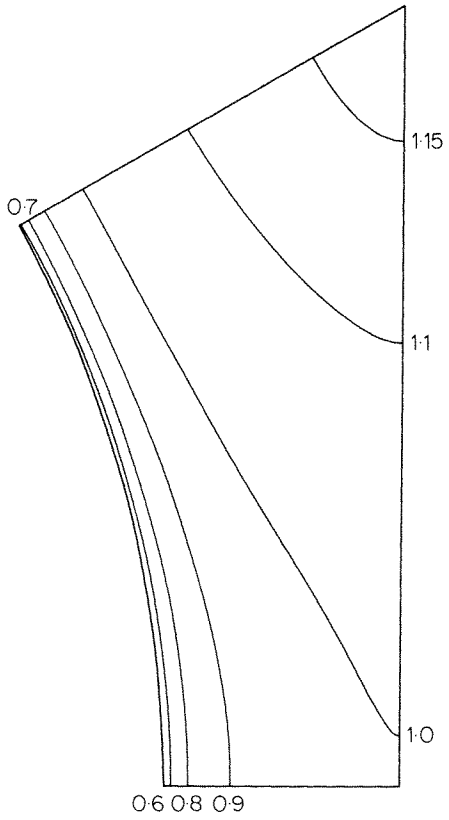

Figure 8. $u/\bar{u}$ contours. $Re = 270\,000$. One equation model length scales equation (12)

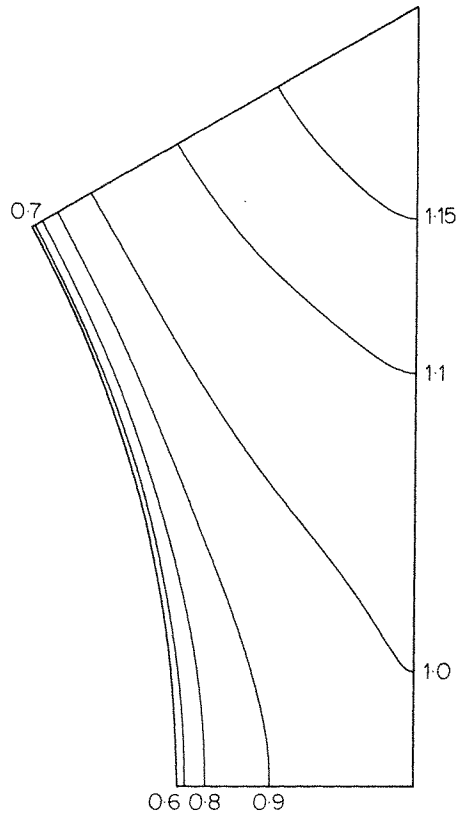

Figure 9. $u/\bar{u}$ contours. $Re = 270\,000$. One equation model length scale from equation (20)

distribution could be obtained using conventional elements to discretise up to the rod surface. The mesh used is shown in Figure 12.

For simplicity it is assumed that g does not vary with position within the rod cross-section so that $g/\bar{g} = 1{\cdot}0$. In addition it is assumed that k_r/k' remains constant at 1·5. In the first instance, eddy viscosity, μ_T/σ_T, is calculated using Buleev's formula.[4] The resulting plot of the temperature distribution is shown in Figure 13. When the one equation model is used to evaluate the turbulent viscosity thus the resulting profile is as shown in Figure 14.

CONCLUSIONS

In general the results obtained for the velocity distribution are better than the corresponding one equation model values. Both sets, however, compare quite favourably with other numerical and experimental data. The wall shear stress, in particular, is quite acceptable. The temperature fields for the coupled fluid/solid system could be obtained quite readily without resorting to the use of associated wall functions which proved to be necessary when solving for the velocity distribution.

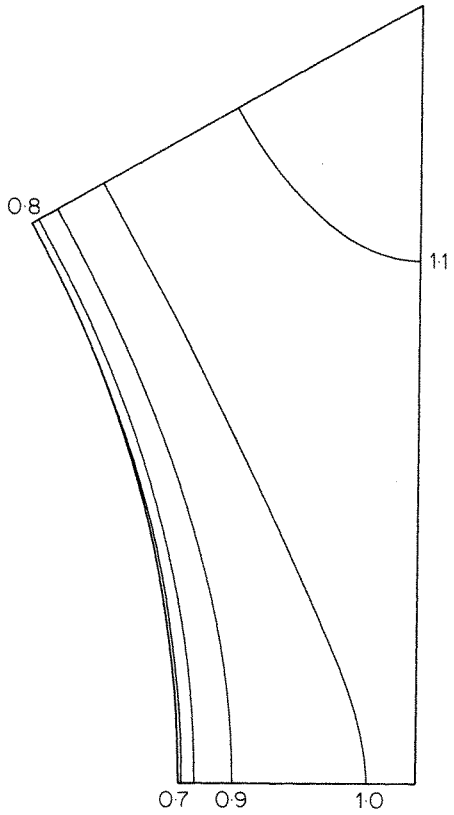

Figure 10. $u/\bar{u}$ contours. $Re = 270\,000$. Two equation model length scale from equation (12)

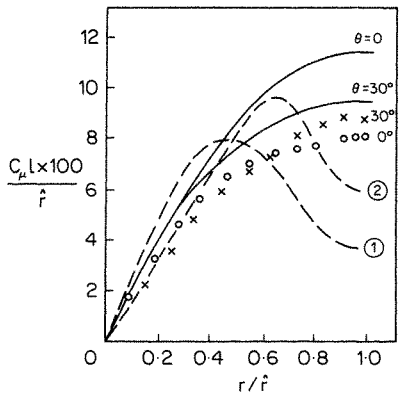

Carajilescov, Todreas[2] ---- ①
Experiment, $\theta = 0°$
Carajilescov, Todreas[2] ---- ②
Experiment, $\theta = 30°$
Buleev[4]

Present work
Two equation model, length scale, $\theta = 0°$ o
Two equation model, $\theta = 30°$ ×

Figure 11. Comparison of two equation model. Length scales

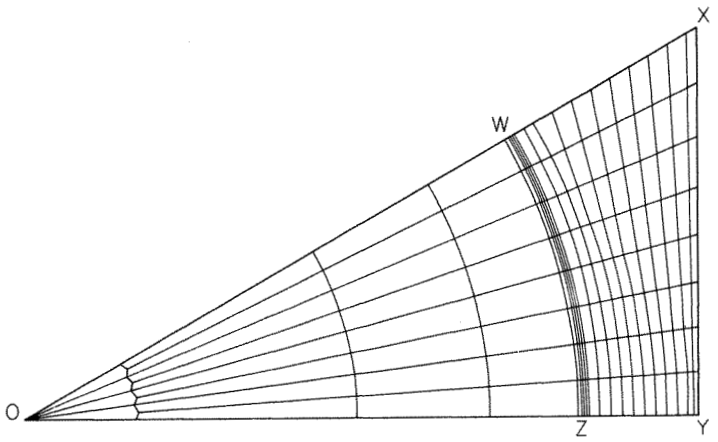

Figure 12. Fine extended mesh, 28 elements in OWZ

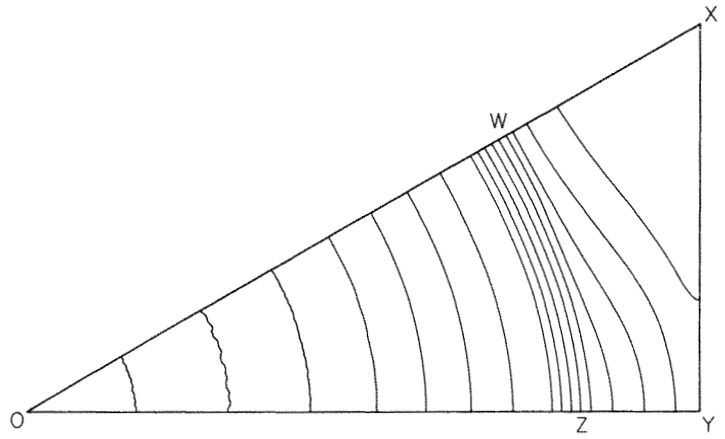

Figure 13. Dimensionless temperature contours with coarse mesh

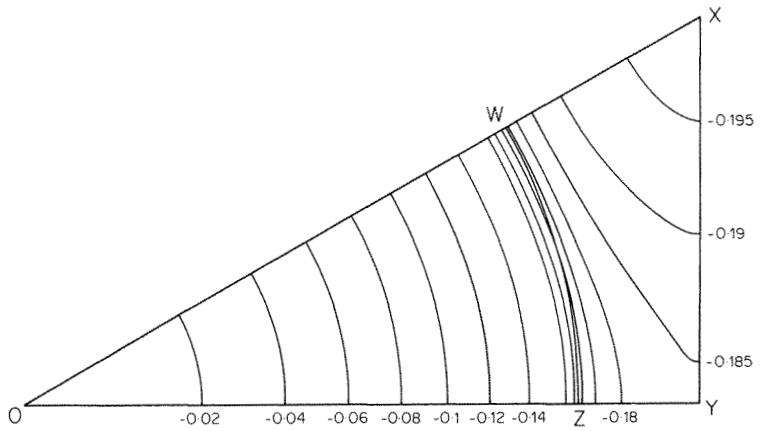

Figure 14. Dimensionless temperature contours, turbulent Prandtl number = 1·4, $k_r/k' = 1{\cdot}5$

REFERENCES

1. R. Meyder, 'Turbulent velocity and temperature distribution in the central sub-channel of rod bundles', *Nucl. Eng. and Design*, **35,** 181–189 (1975).
2. H. Ramm and K. Johannsen, 'A phenomenological turbulence model and its application to heat transport in infinite rod arrays with axial turbulent flow', *J. Heat Trans.*, **97,** 231–237 (1975).
3. N. I. Buleev, 'Theoretical model of the mechanism of turbulent exchange in fluid flows', *A.E.R.E. Translation* by J. J. Cornish, edited by J. Woodrow, 957, 1963.
4. N. I. Buleev and R. Yo. Mironovich, 'Heat transfer in turbulent flow in a triangular array of rods', *Physics and Power Inst.*, Translated from *Teplofizika Vysokohh Temperatur*, **10,** (5) 1031–1038 (1972).
5. R. Nisjing and W. Eifler, 'Axial development of temperature fields in hexagonal fast fuel rod assemblies with liquid metal cooling', *Proc. Int. Mtg. Reactor Heat Transfer*, 252–280, Karlsruhe (1973).
6. P. Carajilescov and N. E. Todreas, 'Experimental and analytical study of axial turbulent flows in an interior sub-channel of a bare rod bundle', *Heat and Mass Transfer, A.S.M.E.*, 262–268, (1976).
7. W. Slager, 'Finite element analysis for turbulent flows of incompressible fluids in fuel rod bundles', *Nucl. Sci. and Eng.*, **66,** 84–92 (1978).
8. M. D. Mikhailov, 'Finite element analysis of turbulent flow heat transfer in rod bundles', *Internal Report.*
9. B. Kjellstrom, 'Studies of turbulent flow parallel to a rod bundle of triangular array', *AE-487*, A.B. Atomenergi, Sweden, 1974.
10. C. Taylor, C. E. Thomas and K. Morgan, 'Analysis of turbulent flow with separation using the F.E.M.', *Computational Techniques in transient and turbulent flow*, Vol. 2 of C. Taylor and K. Morgan, (eds) *Recent Advances in Numerical Methods in Fluids*, Pineridge Press, 1981, pp. 283–325.
11. C. Taylor, C. E. Thomas and K. Morgan, 'F.E.M. and the two equation model of turbulence', in C. Taylor and B. A. Schrefler (eds), *Numerical Methods in Laminar and Turbulent Flow*, Pineridge Press, 1981, pp. 449–462.